BJR

Received: 14 March 2016 | Revised: 9 June 2016 | Accepted: 16 June 2016

http://dx.doi.org/10.1259/bjr.20160242

Cite this article as:
Molina D, Pérez-Beteta J, Luque B, Arregui E, Calvo M, Borrás JM, et al. Tumour heterogeneity in glioblastoma assessed by MRI texture analysis: a potential marker of survival. *Br J Radiol* 2016; **89**: 20160242.

FULL PAPER

Tumour heterogeneity in glioblastoma assessed by MRI texture analysis: a potential marker of survival

[1]DAVID MOLINA, PhD, [1]JULIÁN PÉREZ-BETETA, [1]BELÉN LUQUE, [2]ELENA ARREGUI, MD, [2]MANUEL CALVO, MD, [2]JOSÉ M BORRÁS, MD, PhD, [2]CARLOS LÓPEZ, MD, [3]JUAN MARTINO, MD, PhD, [3]CARLOS VELASQUEZ, MD, [4]BEATRIZ ASENJO, MD, PhD, [4]MANUEL BENAVIDES, MD, PhD, [4]ISMAEL HERRUZO, MD, PhD, [1]ALICIA MARTÍNEZ-GONZÁLEZ, PhD, [5]LUIS PÉREZ-ROMASANTA, MD, PhD, [6]ESTANISLAO ARANA, MD, PhD and [1]VÍCTOR M PÉREZ-GARCÍA, PhD

[1]Instituto de Matemática Aplicada a la Ciencia y la Ingeniería, Universidad de Castilla-La Mancha, Ciudad Real, Spain
[2]Hospital General de Ciudad Real, Ciudad Real, Spain
[3]Hospital Marqués de Valdecilla, Santander, Spain
[4]Hospital Carlos Haya, Málaga, Spain
[5]Hospital Universitario de Salamanca, Salamanca, Spain
[6]Instituto Valenciano de Oncología, Valencia, Spain

Address correspondence to: Dr David Molina
E-mail: *david.molina@uclm.es*

Objective: The main objective of this retrospective work was the study of three-dimensional (3D) heterogeneity measures of post-contrast pre-operative MR images acquired with T_1 weighted sequences of patients with glioblastoma (GBM) as predictors of clinical outcome.
Methods: 79 patients from 3 hospitals were included in the study. 16 3D textural heterogeneity measures were computed including run-length matrix (RLM) features (regional heterogeneity) and co-occurrence matrix (CM) features (local heterogeneity). The significance of the results was studied using Kaplan–Meier curves and Cox proportional hazards analysis. Correlation between the variables of the study was assessed using the Spearman's correlation coefficient.
Results: Kaplan–Meyer survival analysis showed that 4 of the 11 RLM features and 4 of the 5 CM features considered were robust predictors of survival. The median survival differences in the most significant cases were of over 6 months.
Conclusion: Heterogeneity measures computed on the post-contrast pre-operative T_1 weighted MR images of patients with GBM are predictors of survival.
Advances in knowledge: Texture analysis to assess tumour heterogeneity has been widely studied. However, most works develop a two-dimensional analysis, focusing only on one MRI slice to state tumour heterogeneity. The study of fully 3D heterogeneity textural features as predictors of clinical outcome is more robust and is not dependent on the selected slice of the tumour.

INTRODUCTION

Glioblastoma (GBM) is the most frequent malignant brain tumour in adults and the most lethal type, with a median survival of 14.6 months for patients receiving the standard of care, *i.e.* maximal safe surgery plus radiotherapy and chemotherapy.[1] Pre-operative MRI is routinely used for diagnosis, treatment planning, response evaluation and follow-up.

The typical GBM appearance upon diagnosis on MRI consists of an enhanced ring with a central non-enhanced core of necrosis observed mainly on contrast-enhanced T_1 weighted images. Recently, there has been an increased use of advanced imaging techniques alone or in combination with conventional MRI modalities to characterize the connection of the so-called radio phenotype with the tumour genotype, the so-called radiogenomics (*e.g.* recent reviews for GBM[2,3]). However, the use of those techniques requires further research and validation to achieve a broad clinical applicability. Thus, in clinical practice and trials, T_1 contrast-enhanced and T_2/fluid-attenuated inversion-recovery images are still the gold standard for diagnosis and treatment planning.[4]

One of the most important characteristics of GBM is its marked intratumour heterogeneity. In fact, these tumours are usually referred to as "glioblastoma multiforme", in order to highlight their heterogeneous nature. GBM tumours are formed by tumour cells which differ in their morphology, genetics and biological behaviour

and may underlie the inability of conventional therapies to significantly impact patient outcomes.[5] It is well known that heterogeneous tumours are most able to resist treatments like chemotherapy or radiotherapy. Owing to this fact, the study of heterogeneity within the tumour has gained attention in the recent decades.[6]

The purpose of this work was to study the predictive potential of fully three-dimensional (3D) textural heterogeneity measures of post-contrast T_1 weighted MR images in a large data set (resolution, absence of previous treatment). We selected this medical image sequence instead of T_2 or fluid-attenuated inversion recovery owing to its high quality. Textural analysis can be defined as a method for quantifying the spatial distribution of voxel intensities in a set of images. Then, a textural measure is a parameter that characterizes the content of those images. Textural analysis has many applications in a wide number of fields and many different methods have been developed over the recent decades.[7]

Applied to MR tumour images, as the textural features quantify the relationships between voxels, they can be associated with heterogeneity patterns within the segmented volume of the tumour.[8] According to the scale, the heterogeneity parameters can be classified as local, if the relationships considered relate to only pairs of voxels [*e.g.* co-occurrence matrices (CMs)[9]]; regional, if groups of voxels are considered as connected volumes [*e.g.* run-length matrices (RLMs)[7,9]]; or global, if the analysis describes the whole group of images (*e.g.* voxel intensity histograms[10]). These methods have been widely used to analyze lung or breast cancer images.[11–14] However, to our knowledge, only two works have studied two-dimensional (2D) textural features for outcome assessment.[15,16]

METHODS AND MATERIALS

Patients

This retrospective, three-centre (blinded for review) study was approved by the local institutional review boards (blinded for review). All subjects provided written informed consent at hospital admittance for research and treatment. The respective ethical committees approved the study. Patients with pathologically confirmed GBM diagnosed in the period 2006–14 were included in the study. The inclusion criteria were: availability of all the relevant clinical variables [sex, age, type of resection performed, scheme of treatment followed, survival and progression-free survival (PFS)] and availability of pre-operative 3D diagnostic post-contrast T_1 weighted MR images. Exclusion criteria were: (a) multifocal GBMs, (b) tumours with no contrast enhancement, (c) post-contrast-enhanced T_1 weighted MR images that are not in 3D, (d) grid size $< 256 \times 256$ and (e) slice thickness$>$2 mm. 79 cases satisfying the inclusion criteria and not the exclusion criteria were selected. Their main characteristics are summarized in Table 1.

PFS was measured according to the Revised Assessment in Neuro-oncology criteria. Patients who showed no recurrence at the last follow-up were considered as censored events in the PFS Kaplan–Meier analysis. Overall survival (OS) was measured from the time of surgery to the patient's last contact or death. Patients who were still alive at the last follow-up were considered as censored events in the OS Kaplan–Meier analysis.

Image analysis

All MRI examinations were carried out on either 16-channel 1.5 T or32-channel 3 T. Among them, contrast-enhanced 3D T_1

Table 1. Summary of patient characteristics, MRI data and relevant volumetric parameters

Characteristics/parameters	Median or mean value (range)
Patient characteristics	
Median age (interquartile range) (interval) (years)	64 (18) (31, 85)
Sex (%)	36 (45.57) males; 43 (54.43) females
Median survival (interquartile range) (interval) (months)	10.88 (16.17) (0.56, 58.97)
Type of resection (%)	43 (54.43) total resection
	22 (27.85) subtotal resection
	14 (17.72) biopsy
MRI characteristics	
Average pixel spacing (standard deviation) (interval) (mm)	0.88 (0.14) (0.56–1.02)
Average spacing between slices (standard deviation) (interval) (mm)	0.95 (0.12) (0.78, 1.20)
Average slice thickness (standard deviation) (interval) (mm)	1.65 (0.37) (1.00, 2.00)
Average number of slices per patient (standard deviation) (interval)	170.03 (20.26) (124, 202)
Relevant volumetric parameters	
Average 3D tumour volume (standard deviation) (interval) (cm^3)	31.21 (26.73) (0.66, 120.82)
Average 3D contrast-enhancing volume (standard deviation) (interval) (cm^3)	17.73 (15.87) (0.29, 86.33)
Average 3D maximal tumour diameter (standard deviation) (interval) (cm)	4.89 (1.75) (1.37, 11.09)

3D, three-dimensional.

weighted gradient echo sequences were analyzed. Imaging parameters were: voxel size range: 0.97–1.02 mm and gap range: 0.78–1.2 mm. The matrix was 256 × 256 pixels for 68 patients and higher for the remaining cases (range: 448–256 × 448–256 pixels).

Images were processed using a semi-automatic in-house image segmentation program written in the scientific software MATLAB R2015b (The MathWorks, Inc., Natick, MA). It works by dynamically selecting the grey-level value (threshold) which best determines the tumour contour. The resulting segmented tumours were manually corrected by an image analysis expert blinded to clinical information. He was trained by an advisory board consisting of three specialists with more than 10 years' experience in the interpretation of brain MR images (a radiologist, a neurosurgeon and a radio-oncologist).

Owing to the high resolution of MRI data, the segmentation was a time-consuming process, although key for obtaining high-quality results. Results were discussed in consensus readings with the advisory board. To avoid differences in textural analysis due to resolution,[17,18] matrices above 256 × 256 (for 11 patients) were resampled to this resolution. After segmentation, all images were normalized to 32 grey levels following the standard practice in textural analysis.[7] These techniques ensure consistency in terms of contrast and spatial resolution, a common problem in brain tumour imaging.[19]

Heterogeneity measures

A set of 16 classical heterogeneity measures was computed automatically using MATLAB software and added to a database. These measures provide a (local or regional) characterization of the spatial relations between the voxels within the tumour. Our choice of heterogeneity measures is listed in Table A1.

The CM describes the arrangements of pairs of elements (voxels) within 2D images.[11,12,14,20] As it measures relations between only two voxels at a time, it is usually considered to provide information on the local texture of images. Our CM was constructed by including the relationships between voxels in the 13 possible directions in 3D[9] taking only adjacent voxels, *i.e.* considering simultaneously the relations with the 26 neighbours of each voxels in 3D.

The RLM is another standard measure for texture feature extraction.[13] It characterizes large areas within the tumour (groups of voxels) to provide information of regional heterogeneity.[8,9,15,21] Each cell in RLM (i,j) was computed as the number of runs of length j formed by voxels of intensity in box i in all the 13 possible directions in 3D.[9]

Statistical methods

Kaplan–Meier plots and log-rank analysis were used to identify the heterogeneity measures associated with prognosis. A two-tailed significance level (p-value) of $p < 0.05$ was applied. We tried to find measures separating patient populations into two subgroups with significant differences in terms of survival (OS and PFS). To fix the threshold values separating the relevant populations, an optimization strategy was used: (i) the p-values for the full range of thresholds of each heterogeneity feature were computed, (ii) thresholds that separated the populations into reasonably sized subgroups with at least 20 patients were only accepted and (iii) the minimum p-value was selected. In the relevant cases, minima with $p < 0.05$ were found pointing out to relevant regions of the parameter space. For each population split, the hazard ratio as an indicator of risk was computed by using a single-variable Cox proportional hazards regression analysis.

Then, the correlations between the significant variables of the previous analysis were computed in order to identify parameters with similar information. Owing to its non-parametric nature, Spearman's correlation coefficient was considered to study the relation between independent quantitative variables. Correlation coefficient values below 0.1 were taken as indicators of no correlation between the variables while values over 0.7 were taken as indicators of a strong correlation. SPSS software v. 22.0.00 (IBM Corp., New York, NY; formerly SPSS Inc., Chicago, IL) was used for all the statistical analysis.

RESULTS

We segmented and analyzed brain image data sets belonging to the selected 79 patients. Kaplan–Meier curves were constructed for all the variables (taking the mean, median and optimal threshold values to split the patient population into two subgroups). Table 2 and Figure 1 summarize the results obtained.

Overall survival

For OS, the most significant RLM variables of the study were long run emphasis (LRE) ($p = 0.004$) (Figure 1a), high grey-level run emphasis ($p = 0.030$) (Figure 1b), long run high grey-level emphasis (LRHGE) ($p = 0.006$) (Figure 1c) and run percentage (RPC) ($p = 0.001$) (Figure 1d). The increases in the median survival times for the favourable subgroups were 6.71, 6.28, 6.77 and 7.17 months, respectively.

Regarding CM features, the outstanding variables were the entropy ($p = 0.013$) (Figure 1e), homogeneity ($p = 0.018$) (Figure 1f), contrast ($p = 0.013$) (Figure 1g) and dissimilarity ($p = 0.010$) (Figure 1h). The increases in the median survival times for the favourable subgroups were 8.22, 3.42, 5.16 and 6.71 months, respectively.

The thresholds selected in Table 2 are those providing the best results. However, for the most significant variables, there was a large interval of possible significant thresholds. For example, for the RPC, a range of 16 different patient splits were strong predictors of clinical outcome ($p < 0.05$).

Progression-free survival

For PFS, and using the same thresholds, six of the previous eight variables were strongly related to survival: the three RLM features LRE ($p = 0.019$), LRHGE ($p = 0.039$) and RPC ($p = 0.003$) and the three CM features: entropy ($p = 0.044$), contrast ($p = 0.028$) and dissimilarity ($p = 0.046$).

Correlations

Table 3 shows the Spearman's correlation coefficient between every pair of variables. We have also included in this table the

Table 2. Summary of Kaplan–Meier and univariate Cox analysis for the more representative variables

Variables	OS		PFS	
	HR (CI 95%)	*p*-value	HR (CI 95%)	*p*-value
RLM-LRE				
Best: (≤22,000 *vs* >22,000)	**2.034 (1.250, 3.308)**	**0.004**	**1.749 (1.091, 2.803)**	**0.019**
Mean: (≤79,086.80 *vs* >79,086.80)	1.384 (0.821, 2.334)	0.221	1.340 (0.797, 2.253)	0.267
Median: (≤24,524.51 *vs* >24,524.51)	**2.034 (1.250, 3.308)**	**0.004**	**1.749 (1.091, 2.803)**	**0.019**
RLM-HGRE				
Best: (>131 *vs* ≤131)	**1.810 (1.051, 3.116)**	**0.030**	1.592 (0.928, 2.731)	0.088
Mean: (>117.99 *vs* ≤117.99)	1.219 (0.770, 1.929)	0.397	1.131 (0.714, 1.790)	0.599
Median: (>116.51 *vs* ≤116.51)	1.272 (0.803, 2.014)	0.305	1.217 (0.771, 1.921)	0.398
RLM-LRHGE				
Best: (≤940,000 *vs* >940,000)	**1.943 (1.195, 3.158)**	**0.006**	**1.646 (1.021, 2.654)**	**0.039**
Mean: (≤4,438,948.8 *vs* >4,438,948.8)	1.321 (0.799, 2.184)	0.275	1.206 (0.733, 1.985)	0.460
Median: (≤1,412,436.3 *vs* >1,412,436.3)	**1.608 (1.006, 2.571)**	**0.045**	1.396 (0.877, 2.222)	0.157
RLM-RPC				
Best: (>0.068 *vs* ≤0.068)	**2.167 (1.334, 3.519)**	**0.001**	**2.009 (1.248, 3.235)**	**0.003**
Mean: (>0.092 *vs* ≤0.092)	1.585 (0.986, 2.547)	0.055	1.395 (0.871, 2.235)	0.163
Median: (>0.069 *vs* ≤0.069)	**2.011 (1.238, 3.266)**	**0.004**	**1.756 (1.095, 2.816)**	**0.018**
CM-entropy				
Best: (>4.66 *vs* ≤4.66)	**1.815 (1.128, 2.919)**	**0.013**	**1.612 (1.009, 2.574)**	**0.044**
Mean: (>4.52 *vs* ≤4.52)	1.540 (0.970, 2.445)	0.065	1.386 (0.878, 2.189)	0.159
Median: (>4.50 *vs* ≤4.50)	1.442 (0.910, 2.286)	0.117	1.318 (0.835, 2.081)	0.233
CM-homogeneity				
Best: (≤0.49 *vs* >0.49)	**1.789 (1.089, 2.916)**	**0.018**	1.538 (0.952, 2.485)	0.076
Mean: (≤0.47 *vs* >0.47)	1.539 (0.971, 2.441)	0.065	1.320 (0.837, 2.084)	0.230
Median: (≤0.47 *vs* >0.47)	1.539 (0.971, 2.441)	0.065	1.320 (0.837, 2.084)	0.230
CM-contrast				
Best: (>5.20 *vs* ≤5.20)	**1.829 (1.128, 2.965)**	**0.013**	**1.699 (1.054, 2.738)**	**0.028**
Mean: (>7.62 *vs* ≤7.62)	1.180 (0.718, 1.941)	0.513	1.220 (0.743, 2.002)	0.431
Median: (>5.67 *vs* ≤5.67)	1.426 (0.900, 2.261)	0.129	1.286 (0.814, 2.029)	0.279
CM-dissimilarity				
Best: (>1.62 *vs* ≤1.62)	**1.875 (1.155, 3.042)**	**0.010**	**1.612 (1.004, 2.589)**	**0.046**
Mean: (>1.83 *vs* ≤1.83)	**1.635 (1.019, 2.624)**	**0.040**	1.496 (0.934, 2.395)	0.091
Median: (>1.66 *vs* ≤1.66)	1.397 (0.882, 2.214)	0.153	1.211 (0.767, 1.910)	0.410

CI, confidence interval; CM, co-occurrence matrix; HGRE, high grey-level run emphasis; HR, hazard ratio; LRE, long run emphasis; LRHGE, long run high grey-level emphasis; OS, overall survival; PFS, progression-free survival; RLM, run-length matrix; RPC, run percentage.
Bold results correspond to significant results.

correlations of the significant textural features with the patient age, tumour volume and the immunohistochemical proliferation marker Ki67. It is relevant to point out that the CM and RLM 3D features are strongly correlated. The patient age is not correlated with any other parameter while the tumour volume has correlation with almost every significant textural feature.

DISCUSSION

Tumour heterogeneity at the microscopic level is one of the major causes of treatment failure in cancer in general and specifically in GBM.[6] Although heterogeneity in GBM occurs at a molecular scale,[22–24] it is clearly reflected macroscopically in different textures observed in tumour images, both histologically as well as by non-invasive imaging. Hence, textural analysis on GBM MRI T_1

Figure 1. Kaplan–Meier curves for the significant RLM and CM textural features and their respective best threshold included in Table 2. The *p*-value, median difference between the two subgroups and size of each subgroup are provided for each individual case. The triangle mark in the months indicates patients who have survived long. The results shown correspond to the RLM-LRE (a), the RLM-HGRE (b), the RLM-LRHGE (c), the RLM-RPC (d), the CM-Ent (e), the CM-Hom (f), the CM-Con (g) and the CM-Dis (h). CM, co-occurrence matrix; Con, contrast; Dis, dissimilarity; Ent, entropy; HGRE, high grey-level run emphasis; Hom, homogeneity; LRE, long run emphasis; LRHGE, long run high grey-level emphasis; mo, months; RLM, run-length matrix; RPC, run percentage.

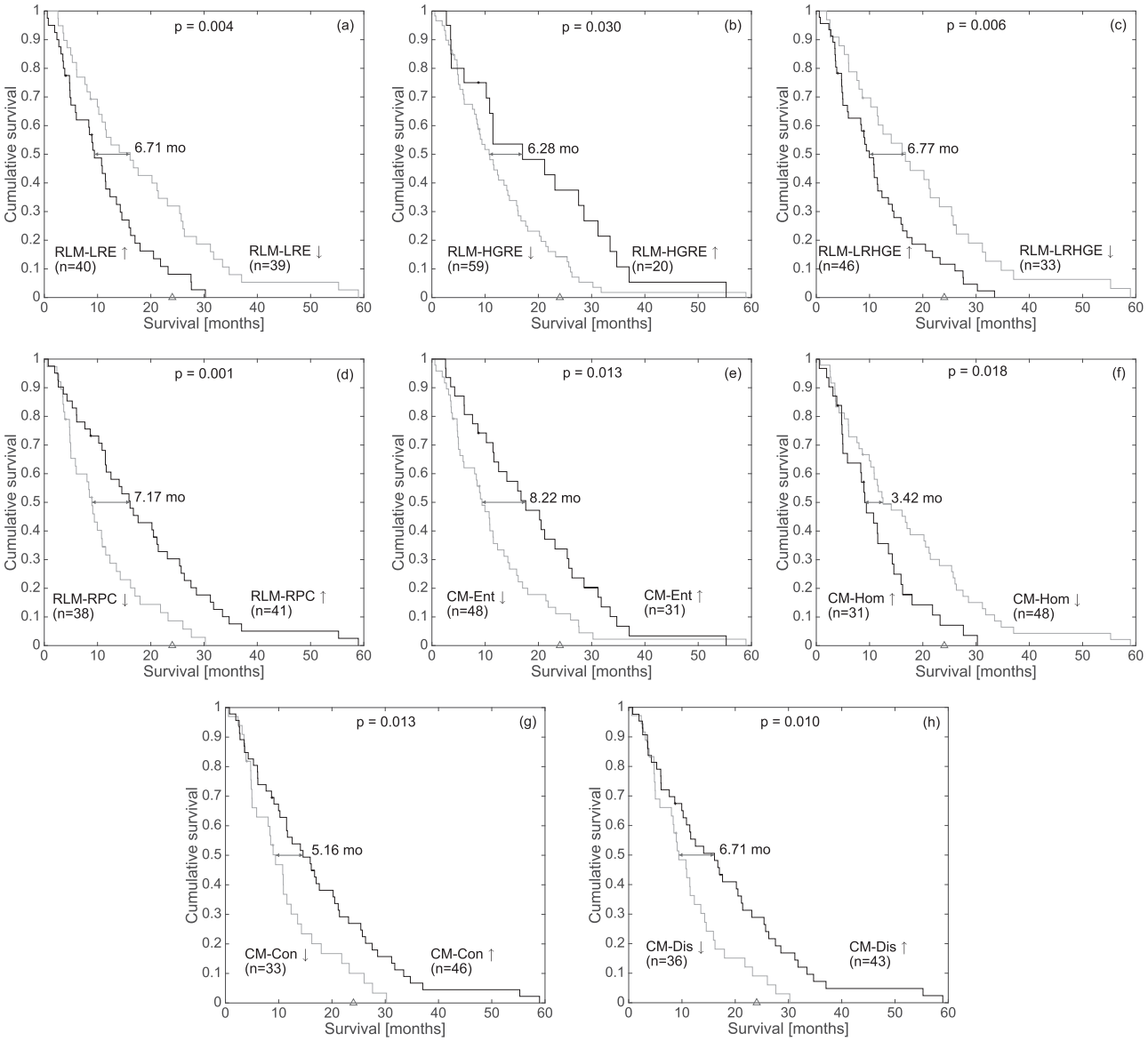

weighted images was used to correlate "macroscopic" heterogeneity with disease outcomes, by means of OS and PFS.

As a non-extensive review of GBM works based on texture analysis, we would like to mention the one by Upadhaya et al,[25] who analyzed data of 40 patients with GBM using 39 textural heterogeneity features on CM and RLM. The objective of their study was to investigate the prognosis value of those textural measures in MR images. Although their study has several limitations,[25] the results suggest that global, regional and local textural features quantifying heterogeneity can provide some prognostic information.

Chaddad et al[24] analyzed 528 CM features (22 features for 24 CM in 2D) of 13 patients with GBM in order to discriminate GBM phenotypes in MR images. Their results demonstrate that texture analysis based on the CM can be helpful in identifying the GBM phenotype.

Some works[26–28] have made use of different textural CM features for the automatic detection and classification of low- and high-grade glioma in MR images. Their results support the hypothesis that the observable heterogeneity in tumours contains information to distinguish gliomas of different grades.

In comparison with previous studies, our data set of 79 patients (i) is larger than that of most of the previous studies (mostly below 50), (ii) includes only high-resolution MRIs (thus reducing noise due to a large voxel size and/or voxel interspacing)

Table 3. Spearman's correlation coefficient (and respective p-value) between the relevant variables of our study

	Age	Volume	Ki67	LRE	HGRE	LRHGE	RPC	CM-Ent	CM-Hom	CM-Con	CM-Dis
Age	**1.00 (0.00)**	−0.17 (0.13)	0.39 (0.11)	−0.04 (0.75)	0.05 (0.65)	0.04 (0.74)	−0.07 (0.54)	−0.01 (0.92)	−0.04 (0.74)	−0.07 (0.57)	−0.02 (0.84)
Volume		**1.00 (0.00)**	−0.01 (0.98)	**0.79 (0.00)**	−0.19 (0.10)	**0.66 (0.00)**	**−0.46 (0.00)**	**−0.44 (0.00)**	**0.60 (0.00)**	**−0.43 (0.00)**	**−0.51 (0.00)**
Ki67			**1.00 (0.00)**	−0.08 (0.76)	0.03 (0.92)	0.07 (7.8)	0.06 (0.81)	−0.01 (0.99)	0.09 (0.73)	−0.00 (0.99)	−0.02 (0.94)
LRE				**1.00 (0.00)**	**−0.36 (0.00)**	**0.92 (0.00)**	**−0.87 (0.00)**	**−0.84 (0.00)**	**0.93 (0.00)**	**−0.85 (0.00)**	**−0.91 (0.00)**
HGRE					**1.00 (0.00)**	−0.19 (0.09)	**0.32 (0.00)**	**0.44 (0.00)**	**0.44 (0.00)**	**0.32 (0.00)**	**0.39 (0.00)**
LRHGE						**1.00 (0.00)**	**−0.92 (0.00)**	**−0.77 (0.00)**	**0.83 (0.00)**	**−0.91 (0.00)**	**−0.90 (0.00)**
RPC							**1.00 (0.00)**	**0.87 (0.00)**	**0.89 (0.00)**	**0.99 (0.00)**	**0.97 (0.00)**
CM-Ent								**1.00 (0.00)**	**−0.94 (0.00)**	**0.90 (0.00)**	**0.94 (0.00)**
CM-Hom									**1.00 (0.00)**	**−0.89 (0.00)**	**−0.96 (0.00)**
CM-Con										**1.00 (0.00)**	**0.98 (0.00)**
CM-Dis											**1.00 (0.00)**

CM, co-occurrence matrix; Con, contrast; Dis, dissimilarity; Ent, entropy; HGRE, high grey-level run emphasis; Hom, homogeneity; LRHGE, long run high grey-level emphasis; LRE, long run emphasis; RPC, run percentage.
Bold results correspond to significant correlations.

and (iii) includes only pre-operative images to avoid post-therapy imaging artefacts/distortions, and (iv) all the analyses are fully 3D on the reconstructed tumours. As in previous works,[24,25,27] we considered together patients with different treatments, as we wanted to relate image heterogeneity with clinical outcome independently of the patient treatment. Although slightly different MRI protocols were used (1.5 T and 3 T), it is well known that changes to MRI sequence parameters are less critical for the outcome of texture analysis than spatial resolution, which may be the most important factor to consider.[17,18]

In this work, we selected a set of classical textural features of local (CM) and regional (RLM) nature. Histograms are also classical tools for heterogeneity computation. However, we did not include histogram features in this work, as we wanted to study the spatial information contained in the tumour.

Kaplan–Meier analysis provided a set of eight heterogeneity measures as significant variables. Five of these measures were more robust in terms of the existence of intervals with broad ranges of threshold values. Specifically, the 3 RLM features LRE, LRHGE and RPC and the 2 CM features entropy and dissimilarity were predictors of survival for >10 different and consecutive patient splits. High values of variables describing tumour homogeneity (homogeneity, LRGHE, LRE) were associated with longer survival groups, while high values of measures of heterogeneity were associated with bad survival (high grey-level run emphasis, RPC, entropy, dissimilarity, contrast).

Interestingly, the significant variables could identify most of the long-term survivors (survival longer than 24 months after diagnosis) in the same group. In Figure 1, we represented this threshold with a triangle mark on the survival axis. It is straightforward to see that most of the heterogeneity features could separate well the long-term survivors.

Table 3 shows strong correlations between 3D CM and RLM features, which point out to redundant information between many of the different heterogeneity measures. Indeed, a detailed observation of Kaplan–Meier curves points out to a similar separation of the patients using different measures. This fact can be due to the 3D analysis developed, which translates into an averaged non-directional mapping of tumour heterogeneity, instead of most standard 2D analyses, where different distances or directions lead to different matrices with partial information.[15,16] However, according to Ng et al,[29] whole-tumour analysis was indeed better than single cross-section analysis in separating the Kaplan–Meier survival curve in colorectal cancer, for which they concluded that whole-tumour analysis seems to be more representative of tumour heterogeneity.[30]

Moreover, among these texture features, entropy is found again, which reflects the unpredictability of the information content of an image. It has been considered to be one of the representative prognostic textural parameters in other tumours.[31]

Thus, one may choose any of these variables as a representative description of tumour heterogeneity applied on MR images acquired with T_1 weighted sequences and use it together with other

more standard clinical features (age, Karnofsky performance status, tumour volume) to define improved metrics of patient prognosis. We would suggest using the two RLM features LRHGE and RPC because of their predictive value in the Kaplan–Meier analysis ($p = 0.006$ and $p = 0.001$, respectively), presence of a high number of thresholds (13 and 16), significantly different survival between the obtained subgroups of patients and their capability to classify most long-term survivors in the best subgroup.

Among advantages, this study is larger than those reported in the literature[32] and reflects the typical patient subgroups that are routinely referred for GBM MRI examinations. Patients were recruited in a multicentre setting, with images from different vendors. However, care was taken to use the same matrix size for textural analysis.

The main interest of the analysis developed in this article is the identification of simple heterogeneity parameters of direct prognostic significance. The subgroup analyses, however, may be underpowered for characterization using heterogeneity features alone owing to data scarcity; therefore, a prospective cohort of patients would most likely be required.

CONCLUSION

We have performed a high-resolution 3D study of GBM heterogeneity in order to verify the prognostic value of different textural features of MRI T_1 weighted post-contrast pre-operative images. The Kaplan–Meyer survival analysis points out the relevance of most of the measures considered as significant predictors of survival and may help in patient selection for surgical intervention. Specifically, patients were found to have better prognosis if their tumour presented a high LRHGE, low RPC, low entropy, high homogeneity or low dissimilarity. We hope that these measures alone or combined could be incorporated into multivariable predictive models of survival for patients with GBM.

ACKNOWLEDGMENTS

We would like to acknowledge Juan Belmonte (Universidad de Castilla-La Mancha) for discussions.

FUNDING

This work has been supported by the Ministerio de Economía y Competitividad/FEDER, Spain (grant numbers: MTM2012-31073 and MTM2015-71200-R), Consejería de Educación Cultura y Deporte from Junta de Comunidades de Castilla-La Mancha, Spain (grant number PEII-2014-031-P), and James S McDonnell Foundation 21st Century Science Initiative in Mathematical and Complex Systems Approaches for Brain Cancer (Special Initiative Collaborative—Planning Grant 220020420 and Collaborative award 220020450).

REFERENCES

1. Stupp R, Mason WP, van den Bent MJ, Weller M, Fisher B, Taphoorn MJ, et al; European Organisation for Research and Treatment of Cancer Brain Tumor and Radiotherapy Groups; ; National Cancer Institute of Canada Clinical Trials Group. Radiotherapy plus concomitant and adjuvant temozolomide for glioblastoma. *N Engl J Med* 2005; **352**: 987–96. doi: http://dx.doi.org/10.1056/NEJMoa043330
2. Ellingson BM. Radiogenomics and imaging phenotypes in glioblastoma: novel observations and correlation with molecular characteristics. *Curr Neurol Neurosci Rep* 2015; **15**: 506. doi: http://dx.doi.org/10.1007/s11910-014-0506-0
3. Zinn PO, Mahmood Z, Elbanan MG, Colen RR. Imaging genomics in gliomas. *Cancer J* 2015; **21**: 225–34. doi: http://dx.doi.org/10.1097/PPO.0000000000000120
4. Wen PY, Macdonald DR, Reardon DA, Cloughesy TF, Sorensen AG, Galanis E, et al. Updated response assessment criteria for high-grade gliomas: response assessment in neuro-oncology working group. *J Clin Oncol* 2010; **28**: 1963–72. doi: http://dx.doi.org/10.1200/JCO.2009.26.3541
5. Bonavia R, Inda MM, Cavenee WK, Furnari FB. Heterogeneity maintenance in glioblastoma: a social network. *Cancer Res* 2011; **71**: 4055–60. doi: http://dx.doi.org/10.1158/0008-5472.CAN-11-0153
6. Inda MM, Bonavia R, Seoane J. Glioblastoma multiforme: a look inside its heterogeneous nature. *Cancers (Basel)* 2014; **6**: 226–39. doi: http://dx.doi.org/10.3390/cancers6010226
7. Xu D, Kurani AS, Furst JD, Raicu DS. Run-length encoding for volumetric texture. *The 4th IASTED international conference on visualization, imaging, and image processing*; 2004. pp. 452–8.
8. Tixier F, Hatt M, Le Rest CC, Le Pogam A, Corcos L, Visvikis D. Reproducibility of tumor uptake heterogeneity characterization through textural feature analysis in 18F-FDG PET. *J Nucl Med* 2012; **53**: 693–700. doi: http://dx.doi.org/10.2967/jnumed.111.099127
9. Tixier F, Le Rest CC, Hatt M, Albarghach N, Pradier O, Metges JP, et al. Intratumor heterogeneity characterized by textural features on baseline 18F-FDG pet images predicts response to concomitant radiochemotherapy in esophageal cancer. *J Nucl Med* 2011; **52**: 369–78. doi: http://dx.doi.org/10.2967/jnumed.110.082404
10. Just N. Improving tumour heterogeneity MRI assessment with histograms. *Br J Cancer* 2014; **111**: 2205–13. doi: http://dx.doi.org/10.1038/bjc.2014.512
11. Ganeshan B, Abaleke S, Young RC, Chatwin CR, Miles KA. Texture analysis of non-small cell lung cancer on unenhanced computed tomography: initial evidence for a relationship with tumour glucose metabolism and stage. *Cancer imaging* 2010; **10**: 137–43. doi: http://dx.doi.org/10.1102/1470-7330.2010.0021
12. Soussan M, Orlhac F, Boubaya M, Zelek L, Ziol M, Eder V, et al. Relationship between tumor heterogeneity measured on FDG-PET/CT and pathological prognostic factors in invasive breast cancer. *PLoS One* 2014; **9**: e94017. doi: http://dx.doi.org/10.1371/journal.pone.0094017
13. Galloway MM. Texture analysis using gray level run lengths. *Comput Vision Graph* 1975; **4**: 172–9. doi: http://dx.doi.org/10.1016/S0146-664X(75)80008-6
14. Haralick RM, Shanmugam K, Dinstein I. Textural features of image classification. *IEEE Trans Syst, Man, Cybern* 1973; **3**: 610–21. doi: http://dx.doi.org/10.1109/TSMC.1973.4309314
15. Chen X, Wei X, Zhang Z, Yang R, Zhu Y, Jiang X. Differentiation of true-progression from pseudoprogression in glioblastoma treated with radiation therapy and

concomitant temozolomide by GLCM texture analysis of conventional MRI. *Clin Imaging* 2015; **39**: 775–80. doi: http://dx.doi.org/10.1016/j.clinimag.2015.04.003

16. Yang D, Rao G, Martínez J, Veeraraghavan A, Rao A. Evaluation of tumor-derived MRI-texture features for discrimination of molecular subtypes and prediction of 12-month survival status in glioblastoma. *Med Phys* 2015; **42**: 6725–35. doi: http://dx.doi.org/10.1118/1.4934373
17. Waugh SA, Lerski RA, Bidaut L, Thompson AM. The influence of field strength and different clinical breast MRI protocols on the outcome of texture analysis using foam phantoms. *Med Phys* 2011; **38**: 5058–66. doi: http://dx.doi.org/10.1118/1.3622605
18. Molina D, Perez-Beteta J, Martinez-Gonzalez A, Arana E, Perez-Garcia VM. Influence of grey level and space discretization on brain tumor heterogeneity measures obtained from MRIs. *Comput Biol Med* 2016. Submitted.
19. Ellingson BM, Bendszus M, Sorensen AG, Pope WB. Emerging techniques and technologies in brain tumor imaging. *Neuro Oncol* 2014; **16**(Suppl. 7): vii12–23. doi: http://dx.doi.org/10.1093/neuonc/nou221
20. Castellano G, Bonilha L, Li LM, Cendes F. Texture analysis of medical images. *Clin Radiol* 2004; **59**: 1061–9. doi: http://dx.doi.org/10.1016/j.crad.2004.07.008
21. Tang X. Texture information in run-length matrices. *IEEE T Image Process* 1998; **7**: 1602–9. doi: http://dx.doi.org/10.1109/83.725367
22. Parker NR, Khong P, Parkinson JF, Howell VM, Wheeler HR. Molecular heterogeneity in glioblastoma: potential clinical implications. *Front Oncol* 2015; **5**: 55. doi: http://dx.doi.org/10.3389/fonc.2015.00055
23. Soeda A, Hara A, Kunisada T, Yoshimura S, Iwama T, Park DM. The evidence of glioblastoma heterogeneity. *Sci Rep* 2015; **27**: 7979. doi: http://dx.doi.org/10.1038/srep07979
24. Chaddad A, Zinn PO, Colen RR. Quantitative texture analysis for glioblastoma phenotypes discrimination. *International Conference on Control, Decision and Information Technologies (CoDIT)*; 2014. pp. 605–8.
25. Upadhaya T, Morvan Y, Stindel E, Le Reste PJ, Hatt M. Prognostic value of multimodal MRI tumour features in glioblastoma multiforme using textural features analysis. *Biomedical Imaging IEEE 12th International Symposium*; 2015. pp. 50–4.
26. Resmi A, Tessamma T. Automatic detection and classification of glioma tumours using statistical features. *Int J Emerging Technol* 2014; **7**: 8–14.
27. Resmi A, Tessamma T. Texture description of low grade and high grade glioma using statistical features in brain MRIs. *Int J Recent Trends Eng Technol* 2010; **4**: 27–33.
28. Ryu YJ, Choi SH, Park SJ, Yun TJ, Kim J-H, Sohn C-H. Glioma: application of whole-tumor texture analysis of diffusion-weighted imaging for the evaluation of tumor heterogeneity. *PLoS One* 2014; **9**: e108335. doi: http://dx.doi.org/10.1371/journal.pone.0108335
29. Ng F, Kozarski R, Ganeshan B, Goh V. Assessment of tumor heterogeneity by CT texture analysis: can the largest cross-sectional area be used as an alternative to whole tumor analysis? *Eur J Radiol* 2013; **82**: 342–8. doi: http://dx.doi.org/10.1016/j.ejrad.2012.10.023
30. Ganeshan B, Miles KA, Young RC, Chatwin CR. Hepatic entropy and uniformity: additional parameters that can potentially increase the effectiveness of contrast enhancement during abdominal CT. *Clin Radiol* 2007; **62**: 761–8. doi: http://dx.doi.org/10.1016/j.crad.2007.03.004
31. Wibmer A, Hricak H, Gondo T, Matsumoto K, Veeraraghavan H, Fehr D, et al. Haralick texture analysis of prostate MRI: utility for differentiating non-cancerous prostate from prostate cancer and differentiating prostate cancers with different Gleason scores. *Eur Radiol* 2015; **25**: 2840–50. doi: http://dx.doi.org/10.1007/s00330-015-3701-8
32. Mackin D, Fave X, Zhang L, Fried D, Yang J, Taylor B, et al. Measuring computed tomography scanner variability of radiomics features. *Invest Radiol* 2015; **50**: 757–65. doi: http://dx.doi.org/10.1097/RLI.0000000000000180

APPENDIX A

Table A1 includes the definition of the heterogeneity measures computed in this study. For CM measures, CM (i,j) stands for the co-occurrence matrix and N is the number of classes of grey levels taken (in this study, 32). For RLM measures, RLM (i,j) is the run-length matrix, n_r is the number of runs, N is the number of classes of grey levels and M is the size in voxels of the largest region found.

Table A1. Definition of the heterogeneity measures computed in this study

Type of measure	Name	Formula
CM	Entropy[14]	$-\sum_{i=1}^{N}\sum_{j=1}^{N}\mathrm{CM}(i,j)\cdot\ln[\mathrm{CM}(i,j)]$
CM	Homogeneity[14]	$\sum_{i=1}^{N}\sum_{j=1}^{N}\frac{\mathrm{CM}(i,j)}{1+(i-j)^2}$
CM	Contrast[25]	$\sum_{i=1}^{N}\sum_{j=1}^{N}\mathrm{CM}(i,j)\cdot(i-j)^2$
CM	Dissimilarity[25]	$\sum_{i=1}^{N}\sum_{j=1}^{N}\mathrm{CM}(i,j)\cdot\lvert i-j\rvert$
CM	Uniformity[11]	$\sum_{i=1}^{N}\sum_{j=1}^{N}[\mathrm{CM}(i,j)^2]^2$
RLM	LRE[7]	$\frac{1}{n_r}\sum_{i=1}^{N}\sum_{j=1}^{M}\mathrm{RLM}(i,j)\cdot j^2$
RLM	SRE[7]	$\frac{1}{n_r}\sum_{i=1}^{N}\sum_{j=1}^{M}\frac{\mathrm{RLM}(i,j)}{j^2}$
RLM	LGRE[7]	$\frac{1}{n_r}\sum_{i=1}^{N}\sum_{j=1}^{M}\frac{\mathrm{RLM}(i,j)}{i^2}$
RLM	HGRE[7]	$\frac{1}{n_r}\sum_{i=1}^{N}\sum_{j=1}^{M}\mathrm{RLM}(i,j)\cdot i^2$
RLM	SRLRE[20]	$\frac{1}{n_r}\sum_{i=1}^{N}\sum_{j=1}^{M}\frac{\mathrm{RLM}(i,j)}{i^2\cdot j^2}$
RLM	SRHGE[20]	$\frac{1}{n_r}\sum_{i=1}^{N}\sum_{j=1}^{M}\frac{\mathrm{RLM}(i,j)\cdot i^2}{j^2}$
RLM	LRLGE[20]	$\frac{1}{n_r}\sum_{i=1}^{N}\sum_{j=1}^{M}\frac{\mathrm{RLM}(i,j)\cdot j^2}{i^2}$
RLM	LRHGE[20]	$\frac{1}{n_r}\sum_{i=1}^{N}\sum_{j=1}^{M}\mathrm{RLM}(i,j)\cdot i^2\cdot j^2$
RLM	GLNU[20]	$\frac{1}{n_r}\sum_{i=1}^{N}\left(\sum_{j=1}^{M}\mathrm{RLM}(i,j)\right)^2$
RLM	RLNU[20]	$\frac{1}{n_r}\sum_{j=1}^{M}\left(\sum_{i=1}^{N}\mathrm{RLM}(i,j)\right)^2$
RLM	RPC[7]	$\frac{n_r}{\sum_{i=1}^{N}\sum_{j=1}^{M}\mathrm{RLM}(i,j)\cdot j}$

CM, co-occurrence matrix; GLNU, grey-level non-uniformity; HGRE, high grey-level run emphasis; LGRE, low grey-level run emphasis; LRE; long run emphasis; LRHGE; long run high grey-level emphasis; LRLGE; long run low grey-level emphasis; RLM, run-length matrix; RLNU, run-length non-uniformity; RPC, run percentage; SRE; short run emphasis; SRHGE, short run high grey-level emphasis; SRLRE, short run low grey-level emphasis.